NASA TECHNICAL NOTE

NASA TN D-5975

NASA TN D-5975

A PREDETECTION POLARIZATION DIVERSITY COMBINER

by Chase P. Hearn

Langley Research Center
Hampton, Va. 23365

NATIONAL AERONAUTICS AND SPACE ADMINISTRATION • WASHINGTON, D. C. • SEPTEMBER 1970

1. Report No. NASA TN D-5975	2. Government Accession No.	3. Reci,
4. Title and Subtitle A PREDETECTION POLARIZATION DIVERSITY COMBINER		5. Report Date September 1970 6. Performing Organization Code
7. Author(s) Chase P. Hearn		8. Performing Organization Report No. L-7057
9. Performing Organization Name and Address NASA Langley Research Center Hampton, Va. 23365		10. Work Unit No. 125-21-05-01 11. Contract or Grant No.
12. Sponsoring Agency Name and Address National Aeronautics and Space Administration Washington, D.C. 20546		13. Type of Report and Period Covered Technical Note 14. Sponsoring Agency Code
15. Supplementary Notes		

16. Abstract

This paper describes the theory, development, and laboratory performance of an experimental polarization diversity combiner. The combiner operates in conjunction with orthogonally polarized S-band antenna feeds and pedestal-mounted downconverters. The system is designed to eliminate effectively the received signal loss caused by polarization mismatch, and will accommodate radiofrequency bandwidths as large as 9 MHz. The use of a multiloop carrier tracking servomechanism for phase-coherent combination of the input signals limits the system application to the class of modulated signals having carriers.

17. Key Words (Suggested by Author(s)) Polarization diversity Diversity combiner	18. Distribution Statement Unclassified – Unlimited		
19. Security Classif. (of this report) Unclassified	20. Security Classif. (of this page) Unclassified	21. No. of Pages 28	22. Price* $3.00

*For sale by the Clearinghouse for Federal Scientific and Technical Information
Springfield, Virginia 22151

A PREDETECTION POLARIZATION DIVERSITY COMBINER

By Chase P. Hearn
Langley Research Center

SUMMARY

This paper describes the theory, development, and laboratory performance of an experimental polarization diversity combiner. The combiner operates in conjunction with orthogonally polarized S-band antenna feeds and pedestal-mounted downconverters. The system is designed to eliminate effectively the received signal loss caused by polarization mismatch, and will accommodate radiofrequency bandwidths as large as 9 MHz. The use of a multiloop carrier tracking servomechanism for phase-coherent combination of the input signals limits the system application to the class of modulated signals having carriers.

INTRODUCTION

Depolarization between spacecraft and earth-based antennas can degrade an otherwise satisfactory communication link. The polarization of an electromagnetic wave received by an earth terminal is dependent on a number of factors: propagation phenomena (Faraday rotation), spacecraft orientation, and geometry as well as transmitting antenna configuration. Choice, or control, of all these factors to guarantee a satisfactory received polarization is not always feasible. For example, a space vehicle which is not stabilized with respect to the earth is generally equipped with a near omnidirectional spacecraft antenna. It is difficult, if not impossible, to maintain a specific polarization over the entire radiation pattern of such antennas; thus, an optimum receiving installation should be polarization adaptive since a receiving antenna exhibits its maximum effective cross-sectional area when it is polarization matched to the incident wave. (See ref. 1.)

An arbitrarily polarized wave may be represented as the vector sum of two spatially orthogonal waves having a fixed time-phase offset. It follows that a wave of arbitrary polarization, being decomposable into orthogonal components, may be received without polarization loss with a pair of orthogonal, linearly polarized antennas (or feeds) provided the components are properly combined. Signals so received cannot be simply added because of the time-phase difference existing between them. This paper is devoted to an examination of what is involved in forming a worthwhile combination of polarization diversity signals, and a description of an experimental polarization diversity system.

Generalized signals as received by a pair of orthogonally polarized antennas (or feeds) might be expressed as

$$s_1(t) = P_1(t)\, A\left[1 + m(t)\right] \sin\left[\omega_o t + \phi(t)\right] \tag{1}$$

$$s_2(t) = P_2(t)\, A\left[1 + m(t)\right] \sin\left[\omega_o t + \phi(t) + \delta(t)\right] \tag{2}$$

in which the $P_1(t)$, $P_2(t)$, and $\delta(t)$ account for those differential aspects of the signals which result in a time-varying received polarization; $m(t)$ and $\phi(t)$ are the message functions.

Additive noise which can stem from sources both internal and external to a ground receiving system is associated with each of these signals. In addition to hindering recovery of $m(t)$ and/or $\phi(t)$, the characteristics of this noise influence considerably the design of a diversity system. For example, a diversity combination which will yield a combined signal-noise ratio (SNR) equal to the sum of the individual SNR values when the channel noises are uncorrelated yields a combined SNR equal to or less than the better of the input SNR values when the channel noises are highly correlated. (See appendix A.) This system was designed for optimum performance with essentially uncorrelated channel noises. Under this condition, predetection combination is preferable to postdetection combination since the combined SNR can be made to exceed either of the input SNR values. Predetection combination, in turn, effectively extends the operating range of detectors subject to thresholding.

It remains to decide which form of diversity combining (selection, equal gain, or maximal ratio) is most appropriate for combining two channels in which the channel noise voltages are uncorrelated. Under these conditions, the optimum weighting scheme was shown by Brennan (ref. 2) to be maximal ratio, in which each channel is gain-weighted directly proportional to the root-mean-square signal voltage and inversely proportional to the mean-square noise voltage in that channel; that is,

$$\frac{G_1(t)}{G_2(t)} = \frac{P_1(t)}{P_2(t)} \frac{N_2}{N_1} \tag{3}$$

This weighting results in a combined SNR equal to the sum of the individual SNR values.

SYMBOLS

A multiplicative factor of received signal amplitude

B_i	phase lock loop input bandwidth
D	ratio of combined signal-noise ratio to sum of input signal-noise ratios
G	gain weighting factor
$F_1(s)$	primary phase lock loop filter transfer function
$F_2(s)$	secondary phase lock loop filter transfer function
f_d	Doppler offset
K_1	primary phase lock loop gain
K_2	secondary phase lock loop gain
m(t)	amplitude message function
N	mean-square noise voltage
n(t)	additive noise voltage
P(t)	polarization-induced fluctuations of received signal amplitude
s	Laplace operator
T	time constant of motor-phase resolver combination
t	time
V	amplitude of received signal
ϵ	phase lock loop steady-state error
λ	dummy variable of integration
ξ	damping ratio
σ	gain weighting error factor

τ	filter time constant
θ_{ch}	horizontal channel phase error
θ_{cv}	vertical channel phase error
θ_{d}	differential phase error
θ_{eh}	horizontal channel composite phase error
θ_{ev}	vertical channel composite phase error
θ_{fh}	horizontal channel feedback phase
θ_{fv}	vertical channel feedback phase
θ_{h}	horizontal channel input phase
θ_{o}	primary loop feedback phase
θ_{r}	reference phase
θ_{s}	phase angle of combined signal
θ_{v}	vertical channel input phase angle
$\phi(t)$	phase message function
δ	differential phase angle
ψ	angular position of phase resolver
ω_{n}	natural resonant frequency
ω_{o}	carrier frequency

Subscripts:

1,2	diversity inputs

i	input
o	output
s	combined value
d	differential value
f	feedback
v	vertical

Abbreviations:

AGC	automatic gain control
AMP	amplifier
AM/PM	amplitude modulation to phase modulation
BW	bandwidth
dc	direct current
H	horizontal
HB	hybrid
HGC	horizontal gain control
IF	intermediate frequency
LO	local oscillator
MR	maximal ratio
PDC	polarization diversity combiner
PLL	phase lock loop

RF	radiofrequency
REF	reference
rms	root mean square
SNR	sound-noise ratio
$(SNR)_{LT}$	sound-noise ratio at loop threshold
V	vertical
VCO	voltage-controlled oscillator
VGC	vertical gain control

Dots denote derivatives with respect to time.

DESCRIPTION OF THE EXPERIMENTAL POLARIZATION DIVERSITY COMBINER

General Description

The basic operations of this system are phase alinement, amplitude weighting, and predetection combining of S-band signals received by a pair of orthogonally polarized antenna feeds. The system accommodates modulated signals which contain discrete carrier components whose amplitudes are independent of the degree of modulation, but dependent on polarization fading through the multiplicative factors P(t). This category includes amplitude and narrow-band angle modulation. The system can effectively combine signals with radiofrequency bandwidths as large as 9 MHz. The system output is at 30 MHz and is used to drive an appropriate data demodulator.

The polarization diversity combiner (PDC) also supplies antenna tracking information through the use of monopulse antenna feeds. Each monopulse channel (vertical and horizontal) supplies three radiofrequency outputs, a sum which has a maximum amplitude when the antenna is on target and two difference outputs whose magnitudes and signs reflect the pointing errors in orthogonal planes.

System operation may be explained with the aid of figure 1, a simplified block diagram of the PDC. The six antenna outputs are preamplified and converted to the first intermediate frequency at 110 MHz in pedestal-mounted front ends. The local oscillator

signal for this mixing is derived from a frequency standard which also supplies (phase) reference signals for the remaining sections of the PDC.

At the inputs to the second mixers, the monopulse sum signals enter a dual input multiloop servomechanism which brings the received carriers into phase coherence, performs maximal ratio (MR) gain weighting, and develops an AGC common to all IF amplifiers. (Throughout these operations the monopulse difference channels are slaved to the sum channel.)

The above-mentioned operations are all dependent on the carrier tracking loops being locked. Initial acquisition is facilitated with a frequency lock loop which can correct for first local oscillator tuning errors up to ±50 kHz.

The idea of using the MR combination in conjunction with a multiloop carrier tracking servo as the basis of an effective diversity system is not new. (See ref. 3.) Up to the present time only a few applications of this scheme have been publicized. (See refs. 4 and 5.) A unique aspect of this system is the large predetection bandwidth of 9 MHz as compared with 300 kHz or less in earlier combiners.

Carrier Tracking Loops

Samples of the (monopulse) sum channel signals (horizontal and vertical) are taken prior to the gain weighting stages and routed to the polarization sensor. These signals are compared with a reference signal to develop an error voltage proportional to $(\theta_v - \theta_r)$ and $(\theta_h - \theta_r)$. The combined signal is also compared with an identical phase reference in the carrier detector to develop an error proportional to $(\theta_s - \theta_r)$. The three error signals are then negatively fed back through the second local oscillator. Thus, a primary phase lock loop (PLL) tracks the average phase of the combined vertical and horizontal inputs and two secondary loops, in effect, track the phase differential between the two input signals.

The carrier tracking loop is analyzed and its operational characteristics are discussed in detail in appendix C. In summary, the primary PLL is of second order, and is capable of tracking frequency ramps up to 0.7 kHz/second, or one-tenth of the anticipated maximum Doppler rate. The remaining Doppler rate and offset are compensated for by supplying programed inputs (based on estimates of the flight trajectory) to the loop. The secondary loops are of first order and are designed to track rates of change of phase up to 2π radians/second. These numbers are based on tracking an Apollo type space vehicle and could easily be changed to accommodate a spin-stabilized spacecraft; however, the secondary loop bandwidths are limited to perhaps a hundred times those used here because of time-response limitations inherent to the electromechanical phase shifters (motor-driven resolvers) which are used in these loops.

Common Automatic Gain Control Gain Weighting

A common AGC loop holds the magnitude of the carrier component of the combined signal essentially constant. The AGC signal is developed by a correlation detector followed by an integrator. All IF amplifiers prior to the point at which the polarization sensor samples the vertical and horizontal channels are (gain) controlled by this AGC signal. The vertical and horizontal channels have equal gain up to the point at which gain weighting takes place; hence, MR combination may be achieved without weighting with noise power ratio (matched vertical and horizontal channels being assumed). The actual gain weighting is accomplished with voltage-controlled attenuators which employ hot carrier diodes as voltage-variable resistance elements in a symmetrical π configuration. The actuating signals for these attenuators are derived in the polarization sensor and their ratio is proportional to the ratio of the carrier amplitudes in the vertical and horizontal channels.

Subsystem Matching

Satisfactory operation of this PDC is highly dependent on gain and phase matching between corresponding components (front ends, IF amplifiers, bandpass filters, and so forth) in the vertical and horizontal channels, particularly the monopulse sum channels. No problems were experienced in satisfactorily matching both gain and phase with respect to frequency; however, amplifier AGC characteristics and limiter amplitude-phase characteristics were more difficult to match. The first problem was alleviated but not eliminated by using a combination of fixed dc bias and resistive padding to effect a closer match between amplifier AGC characteristics. In retrospect, a much better approach would be to use fixed gain amplifiers with voltage-controlled attenuators for gain control. The attenuators used for MR weighting were easily matched to within 3 percent for a 20-dB control range.

Differential phase shift between limiters occurred when the input signals differed in amplitude. Series diode clipper sections were found to be far superior to either shunt diode or emitter coupled pair limiters with respect to AM/PM conversion. The final circuit showed less than 6^{o} differential phase shift for a 20-dB input amplitude inbalance.

EVALUATION AND PERFORMANCE OF THE PDC

This section presents experimental data which describe the performance of various PDC subsystems and the overall system. The more salient characteristics of the system are shown in table I.

Aside from the rather high noise figure, the RF downconverters did not significantly degrade the systems performance. Thus, the following discussion is concerned with the IF combiner performance. The measurements to be discussed were made in the

monopulse sum channels by using the setup shown in figure 2. In all cases to be discussed, the tracking loops were initially locked to the 110-MHz carrier signal.

TABLE I.- SALIENT PDC OPERATIONAL CHARACTERISTICS

Six channel downconverter:	
Input frequency, GHz	2.290 to 2.300
RF bandwidth, MHz	50
Noise figure, dB	5
Gain matching, dB over a 20-MHz bandwidth	0.1
Phase matching, degrees over a 20-MHz bandwidth	5
Local oscillator	Coherent decade frequency synthesizer; switch selectable in 1-kHz steps
IF combiner:	
Input frequency, MHz	110
Noise figure, dB	7
IF bandwidth, MHz	9
IF phase linearity, degrees across IF bandwidth	±10
Tracking bandwidths:	
Primary loop, Hz/sec	700
Secondary loops, rad/sec	2π
Tracking sensitivity (primary loop), dBm	-140
Phase matching, degrees over frequency and dynamic range	≦6
Gain matching, dB over frequency and dynamic range	≦3.5
Dynamic range, dB	60
IF output, MHz	30
Overall combining efficiency (equal input signals), dB	≧2.3

Gain and Phase Match as Functions of Input Signal Amplitude

By using only the carrier source, equal-amplitude 110-MHz input signals were applied to the combiner and the differential gain and phase errors measured at the final IF summing junction. Equal-amplitude input signals were used because it is under this condition that the combiner performance is most seriously degraded. (See appendix B.) These data, plotted in figures 3 and 4, show maximum gain and phase errors of 3.5 dB and 6^{o}, respectively, over a 60-dB dynamic range. These errors can cause a maximum degradation of 0.3 dB from an ideal summation. (See eq. (B3).)

Differential Gain and Phase Match as Function of Frequency

A carrier level of -100-dBm and -70-dBm test signals from the signal generator were applied to the combiner. Gain and phase errors in the combined test signal were measured at the final summing junction. From figures 5 and 6 and equation (B3), these errors cause a maximum degradation of 0.1 dB from an ideal combination.

Weighting Accuracy as Function of Input Signal Amplitude Ratio

The weighting accuracy was checked by applying a known input signal ratio from the carrier source and measuring the ratio of these signals at the final summing junction. Ideally, the ratio of MR combined signals is the square of the ratio of the input signals. These data are plotted in figure 7.

Sound-Noise Ratio Improvement With Equal-Amplitude Input Signals

As a final measure of combiner performance, equal-amplitude test signals were applied and SNR enhancement between the inputs and the output of the final summing junction determined as a function of frequency, with carrier level a parameter. These data are plotted in figure 8 and show a minimum SNR enhancement of approximately 2.3 dB over frequency and dynamic range. The data points at a carrier level of -130 dBm are of questionable accuracy in that they show a 3.2-dB SNR enhancement – an impossibility. These errors were introduced by a poor measurement procedure which became increasingly inaccurate as the input signal amplitudes were reduced.

CONCLUDING REMARKS

The results of this paper are primarily of a practical nature. Specifically, the feasibility of a wide predetection bandwidth (9 MHz) polarization diversity combiner has been demonstrated. Various sources of system error have been examined and their characteristics described for an experimental polarization diversity combiner and techniques for reducing certain of these errors were suggested. With all sources of error, the system exhibits a signal-noise ratio enhancement of at least 2.3 dB. When used in conjunction with orthogonal monopulse feeds, the receiving system is polarization adaptive. The most fundamental limitation of the system is perhaps its inability to track modulated signals lacking carriers such as wide-band frequency and single side-band modulation.

Langley Research Center,
National Aeronautics and Space Administration,
Hampton, Va., June 8, 1970.

APPENDIX A

MAXIMAL RATIO COMBINATION

The purpose of this appendix is to present a simple derivation of the maximal ratio weighting relationship along the lines of that published by Kahn. (See ref. 6.) Figure 9 represents a basic polarization diversity combiner in which sinusoidal input signals are assumed to be maintained in phase coherence by phase-control circuitry. These signals are assumed to be corrupted by internal (hence, uncorrelated between channels) bandpass noise.

The output voltage signal-noise ratio is

$$\frac{s_o(t)}{n_o(t)} = \frac{\left(\sqrt{2}G_1V_1 + \sqrt{2}G_2V_2\right)\sin \omega_o t}{G_1n_1(t) + G_2n_2(t)} \tag{A1}$$

Because of the assumed phase coherence of the signals and incoherence of the noise voltages, the combined power SNR may be written as

$$(SNR)_o = \frac{G_1^2V_1^2 + 2G_1G_2V_1V_2 + G_2^2V_2^2}{G_1^2N_1 + G_2^2N_2} \tag{A2}$$

This expression has a maximum with respect to G_1/G_2 when

$$\frac{G_1}{G_2} = \frac{V_1}{V_2}\frac{N_2}{N_1} \tag{A3}$$

For this gain ratio, the SNR is

$$SNR = \frac{V_1^2}{N_1} + \frac{V_2^2}{N_2} \tag{A4}$$

or the sum of the individual SNR values.

A much different result is obtained if the channel noise voltages are essentially correlated (between channels) as would occur if the noise was predominantly external in origin. Equation (A2) now reads

$$(SNR)_o = \frac{\left(G_1V_1 + G_2V_2\right)^2}{\left(G_1\sqrt{N_1} + G_2\sqrt{N_2}\right)^2} \tag{A5}$$

since the noise voltages add directly. In this case, the output SNR resulting from a MR combination is actually less than the better of the two input SNR values. To show this relationship, equation (A5) is normalized to $(SNR)_1$ with G_1/G_2 being given by equation (A3)

$$\frac{(SNR)_o}{(SNR)_1} = \frac{\left[1 + \frac{(SNR)_2}{(SNR)_1}\right]^2}{\left[1 + \sqrt{\frac{(SNR)_2}{(SNR)_1}}\right]^2} \tag{A6}$$

which has a minimum value of 0.685 when $\frac{(SNR)_2}{(SNR)_1} = 0.171$, or 1.7 dB less than the larger input SNR. Switching diversity is clearly preferable to maximal ratio diversity when the channel noises are highly correlated.

APPENDIX B

ERROR ANALYSIS OF A NONIDEAL MAXIMAL RATIO COMBINATION

For the nonideal maximal ratio combination of figure 10, the degradation of output power SNR relative to an ideal combination as a function of amplitude weighting error σ and phase error δ can be determined. As before, the input signals are sinusoids of amplitudes $V_1\sqrt{2}$ and $V_2\sqrt{2}$. The noise voltages are assumed to be uncorrelated and of equal mean-square value. The last two conditions are approximately met in the PDC, where a common AGC voltage controls precombination gain in all channels.

The output power SNR in an arbitrary bandwidth about ω_o is

$$(SNR)_o = \frac{\left[V_1G_1 + V_2G_2(1 + \sigma)\cos\delta\right]^2 + \left[V_2G_2(1 + \sigma)\sin\delta\right]^2}{N\left[G_1^2 + G_2^2(1 + \sigma)^2\right]} \tag{B1}$$

The mean-square channel noises being equal, the optimum gain ratio G_1/G_2 is, from equation (A3),

$$\frac{G_1}{G_2} = \frac{V_1}{V_2} \tag{B2}$$

for the ideal coherent summation. By using this information, equation (B1) may be normalized to the sum of the input SNR values

$$\frac{(SNR)_o}{(SNR)_1 + (SNR)_2} = D\left(\sigma, \frac{V_2}{V_1}, \delta\right) = \frac{1 + 2\left(\frac{V_2}{V_1}\right)^2(1 + \sigma)\cos\delta + \left(\frac{V_2}{V_1}\right)^4(1 + \sigma)^2}{\left[1 + \left(\frac{V_2}{V_1}\right)^2\right]\left[1 + \left(\frac{V_2}{V_1}\right)^2(1 + \sigma)^2\right]} \tag{B3}$$

The behavior of this equation around the optimum point $\sigma = 0$, $\delta = 0$ is of interest. It may be seen from table II that D decreases most rapidly with σ,δ when the input signals are of equal amplitude.

TABLE II.- SNR DEGRADATION WITH GAIN AND PHASE ERRORS

Case	Phase error, δ	Gain error, σ	V_2/V_1	D	D, dB
1	$\pm 60^o$	0	1	0.75	1.25
2	0	+1, -1/2	1	.90	.45
3	$\pm 60^o$	+1, -1/2	1	.70	1.54
4	$\pm 60^o$	0	2	.761	1.18
5	$\pm 60^o$	+1	2	.767	1.15
6	$\pm 60^o$	-1/2	2	.70	1.54

It is worth noting in the unequal signal cases (cases 4 to 6) that gain and phase errors can be partially compensating. In general, $\frac{\partial D}{\partial (V_2/V_1)}$ equals zero, and thus indicates a maximum or minimum of D, when

$$(1 + \sigma)2\left(\frac{V_2}{V_1}\right)^2 \cos \delta - (1 + \sigma)\left[\left(\frac{V_2}{V_1}\right)^2 - 1\right] + \cos \delta = 0 \qquad \text{(B4)}$$

is satisfied.

APPENDIX C

TRACKING LOOP ANALYSIS

Basic Equations

This section examines the carrier tracking servomechanism for the purpose of deriving equations describing its behavior. The analysis considers the case of equal input signals because it is under this condition that the MR combination is most seriously degraded by noncoherence between the combined signals. (See appendix B.)

Only the sum channel needs to be considered since the difference channels are slaved to the sum channel. Figure 11 was derived from the overall block diagram. It contains only elements which are essential to this analysis and serves as an intermediate step in the development of a phase equivalent circuit. An idealized phase transfer function for the motor-driven resolvers in figure 11 may be derived by noting that in the vertical channel

$$\theta_{fv}(t) = \theta_o(t) + \psi_v(t) \tag{C1}$$

where $\psi_v(t)$ is the angular position of the resolver shaft. The angular velocity of the dc motor $d\psi_v/dt$ is assumed to be proportional to the phase error $\theta_{cv}(t)$:

$$\frac{d\psi_v}{dt} = \theta_{cv}(t) \tag{C2}$$

therefore,

$$\theta_{fv}(t) = \theta_o(t) + \int_0^t \theta_{cv}(\lambda)d\lambda \tag{C3}$$

or in transform notation,

$$\theta_{fv}(s) = \theta_o(s) + \frac{1}{s}\,\theta_{cv}(s) \tag{C4}$$

Similar equations can be derived for the horizontal channel. Time-response limitations of the dc motor necessitate a slight modification of the expression which will be introduced later. The IF signal summer acts as a phase averager to equal-amplitude input signals. With these preliminaries the phase equivalent circuit (fig. 12) follows logically. No generality is lost in assuming $\theta_r(s)$, the reference phase, to be zero. From figure 12,

$$\theta_s(s) = \frac{\theta_{eh}(s) + \theta_{ev}(s)}{2} \tag{C5}$$

The vertical and horizontal composite phase errors, $\theta_{ev}(s)$ and $\theta_{eh}(s)$, may each be viewed as consisting of two parts: the combined phase error $\theta_s(s)$, and the deviation from the average $\theta_d(s)$. However, $\theta_d(s)$ does not appear as an isolated signal in the system

$$\theta_{ev}(s) = \theta_s(s) + \theta_d(s) \tag{C6}$$

and

$$\theta_{eh}(s) = \theta_s(s) - \theta_d(s) \tag{C7}$$

The differential phase error is, from equations (C6) and (C7),

$$\theta_d(s) = \frac{\theta_{ev}(s) - \theta_{eh}(s)}{2} \tag{C8}$$

Thus, $\theta_{ev}(s)$ may be shown to be

$$\theta_{ev}(s) = \frac{s\theta_v(s) - \theta_s(s)\, K_1F_1(s)}{s + K_2F_2(s)} \tag{C9}$$

and

$$\theta_{eh}(s) = \frac{s\theta_h(s) - \theta_s(s)\, K_1F_1(s)}{s + K_2F_2(s)} \tag{C10}$$

Substituting equations (C9) and (C10) in equations (C5) and (C8) yields

$$\theta_d(s) = \frac{\theta_v(s) - \theta_h(s)}{2} \frac{s}{s + K_2F_2(s)} \tag{C11}$$

and

$$\theta_s(s) = \frac{\theta_v(s) + \theta_h(s)}{2} \frac{s}{s + K_1F_1(s) + K_2F_2(s)} \tag{C12}$$

which define the differential and average phase errors in terms of the input phase angles and loop parameters. The second factor in equation (C12) is also the transfer function of the system to the phase of the combined input signals.

Selection of the Loop Filters

The loop filters $F_1(s)$ and $F_2(s)$ are dictated by the anticipated behavior of $\frac{\theta_v + \theta_h}{2}$, $\frac{\theta_v - \theta_h}{2}$, and the errors that can be tolerated in tracking these inputs. At S-band, axial-motion effects between spacecraft and ground antennas appear to be the most important considerations in selecting the primary loop filter. Doppler frequency offsets as large as 80 kHz and Doppler shifts up to 7 kHz/second are to be expected.

These parameters may be predicted from the flight trajectory since it is usually well defined. Thus, the loop may be designed either to track f_d and $\dot{f}_d$ to their maximum excursions or programed inputs derived from the flight trajectory can be supplied to the loop that largely compensate for f_d and $\dot{f}_d$. The later course was followed and the primary loop made of second order, type 1, capable of tracking frequency ramps up to one-tenth of the maximum anticipated Doppler shift or 0.7 kHz/second.

The behavior of the differential phase input $\frac{\theta_v - \theta_h}{2}$ seems to be more difficult to predict, since it is dependent on the spacecraft's antenna characteristics and spatial orientation with respect to the receiving antenna. The rate at which a manned space vehicle can change orientation is very slow. The most drastic maneuver is probably a roll or tumble. For example, the Apollo spacecraft is limited operationally to a maximum roll rate of perhaps 10^o per second. The rate at which the polarization of a wave received from a spacecraft changes as the spacecraft undergoes a tumble was assumed to be rather rapid compared with the roll rate, and the secondary loops were designed to track rates of change of phase, due to $\delta(t)$, up to 2π radians/second.

To accommodate phase ramp inputs with finite tracking errors requires that the secondary loops be first order, type 1, corresponding to an $F_2(s) = 1$ in equation (C11). In this system it is necessary to include with $F_1(s)$ a factor which accounts for time response limitations of the dc motor-phase resolver combination. Equation (C4), which describes the operation of the combination, is more accurately given by

$$\theta_{fv}(s) = \theta_o(s) + \frac{\theta_{cv}(s)}{s(sT + 1)} \tag{C13}$$

where T is the time constant of the elements and was found experimentally to be 4 milliseconds. Taking the lag term into account modifies the expression for differential phase error (eq. (C11)) to

$$\theta_d(s) = \frac{s(sT + 1)}{s^2T + s + K_2} \frac{\theta_v(s) - \theta_h(s)}{2} \tag{C14}$$

Application of the final value theorem (ref. 7, p. 147)

$$\epsilon_o = \lim_{t\to\infty} \theta_d(t) = \lim_{s\to 0} s\theta_d(s) \tag{C15}$$

to equation (C14) yields the steady-state error. For a phase ramp input

$$\frac{\theta_v(s) - \theta_h(s)}{2} = \frac{2\pi}{s^2}$$

hence

$$\epsilon_d = \frac{2\pi}{K_2} \tag{C16}$$

It was desired to limit this error to 0.25 radian, a value at which a sinusoidal phase detector, the most nonlinear element in the loop, departs from linearity by about 1 percent. The required gain K_2 is therefore 25. At this gain the secondary loop is for all practical purposes independent of the lag term $(0.004s + 1)^{-1}$ and it will be neglected in all that follows.

A transfer function that closely approximates

$$F_1(s) = \frac{s\tau_2 + 1}{s\tau_1} \tag{C17}$$

was used in the primary loop. The combined phase error (eq. (C12)) is, with this loop filter,

$$\theta_s(s) = \frac{s^2}{s^2 + s\left(K_2 + \frac{K_1\tau_2}{\tau_1}\right) + \frac{K_1}{\tau_1}} \frac{\theta_v(s) + \theta_h(s)}{2} \tag{C18}$$

which may be put in the standard notation of a second-order servomechanism

$$\theta_s(s) = \frac{s^2}{s^2 + 2\xi\omega_n s + \omega_n^2} \frac{\theta_v(s) + \theta_h(s)}{2} \tag{C19}$$

Application of the final-value theorem to equation (C19) yields, for a phase parabola input $\dot{\omega}/s^3$, the static error

$$\epsilon_S = \frac{\dot{\omega}}{\omega_n^2} \tag{C20}$$

The dynamic characteristics of the loop are determined by both ω_n and ξ. A damping factor of 0.707 results in a reasonable compromise between the conflicting factors of rise time and overshoot for a phase parabola input (ref. 8, pp. 34-35); furthermore, $\xi = 0.707$ has been shown to be optimum for tracking a noise-corrupted phase parabola input (ref. 8, p. 72). With ϵ_S, ξ, and K_2 known, ω_n, τ_2, and K_1/τ_1 may be determined from equations (C18), (C19), and (C20) and are: $\omega_n = 133$ (for $\dot{\omega} = 2\pi \times 700$ radians/second^2), $\tau_2 = 9.2 \times 10^{-3}$, and $K_1/\tau_1 = 1.76 \times 10^4$.

There are sound practical and theoretical justifications for preceding a PLL with a bandpass limiter. (See ref. 8, p. 73.) In designing a prelimited loop, it is necessary to consider the signal suppression effect which becomes important when the input SNR to the limiter is less than 10. For $(SNR)_i < 10$, the effective loop gain decreases with decreasing $(SNR)_i$. In terms of the loop parameters already specified, it may be shown that the minimum $(SNR)_i$, which occurs at loop threshold $(SNR)_{LT}$, is given by (ref. 8, p. 20)

$$(SNR)_{iT} = \frac{\omega_n}{B_i} \frac{\xi + 1}{4\xi} (SNR)_{LT} \tag{C21}$$

The input filter bandwidth B_i was set at 3 kHz to accommodate the tracking error of the frequency lock loop. Taking a conservative 10 as $(SNR)_{LT}$ leads to a value of unity for $(SNR)_{iT}$. At this SNR the limiter suppression factor is approximately 0.66. (See ref. 8, p. 56.) At loop threshold the loop gain is therefore 0.66 of the gain at high values of $(SNR)_i$. Threshold was taken as the design point for ξ and ω_n. At high input SNR values, ω_n increases to 165 and ξ to 0.883. These changes are relatively insignificant in terms of loop performance.

Stable operation of the multiloop servo is assured since the poles of equations (C14) and (C18) lie well in the left half-plane for values of gain K_1 and K_2 far in excess of the design values.

REFERENCES

1. Hartop, R. W.: Power Loss Between Arbitrarily Polarized Antennas. Tech. Rept. No. 32-457 (Contract No. NAS 7-100), Jet Propulsion Lab., C.I.T., Sept. 1, 1964.

2. Brennan, D. G.: Linear Diversity Combining Techniques. Proc. IRE, vol. 47, no. 6, June 1959, pp. 1075-1102.

3. Laughlin, C. R.: The Diversity-Locked Loop – A Coherent Combiner. IEEE Trans. Space Electron. Telemetry, vol. SET-9, no. 3, Sept. 1963, pp. 84-92.

4. Taylor, Ralph E.: Satellite Tracking Simultaneous-Lobing Monopulse Receiving System With Polarization Diversity Capability. IEEE Trans. Aerosp. Electron. Syst., vol. AES-3, no. 4, July 1967, pp. 664-680.

5. DiLosa, V. J.: Diversity-Lock Phase Demodulator. NASA TN D-3342, 1966.

6. Kahn, L. R.: Ratio Squarer, Proceedings IRE, vol. 42, no. 11, Nov. 1954, p. 1704.

7. Van Valkenburg, M. E.: Network Analysis. Prentice-Hall, Inc., c.1955.

8. Gardner, Floyd M.: Phaselock Techniques. John Wiley & Sons, Inc., c.1966.

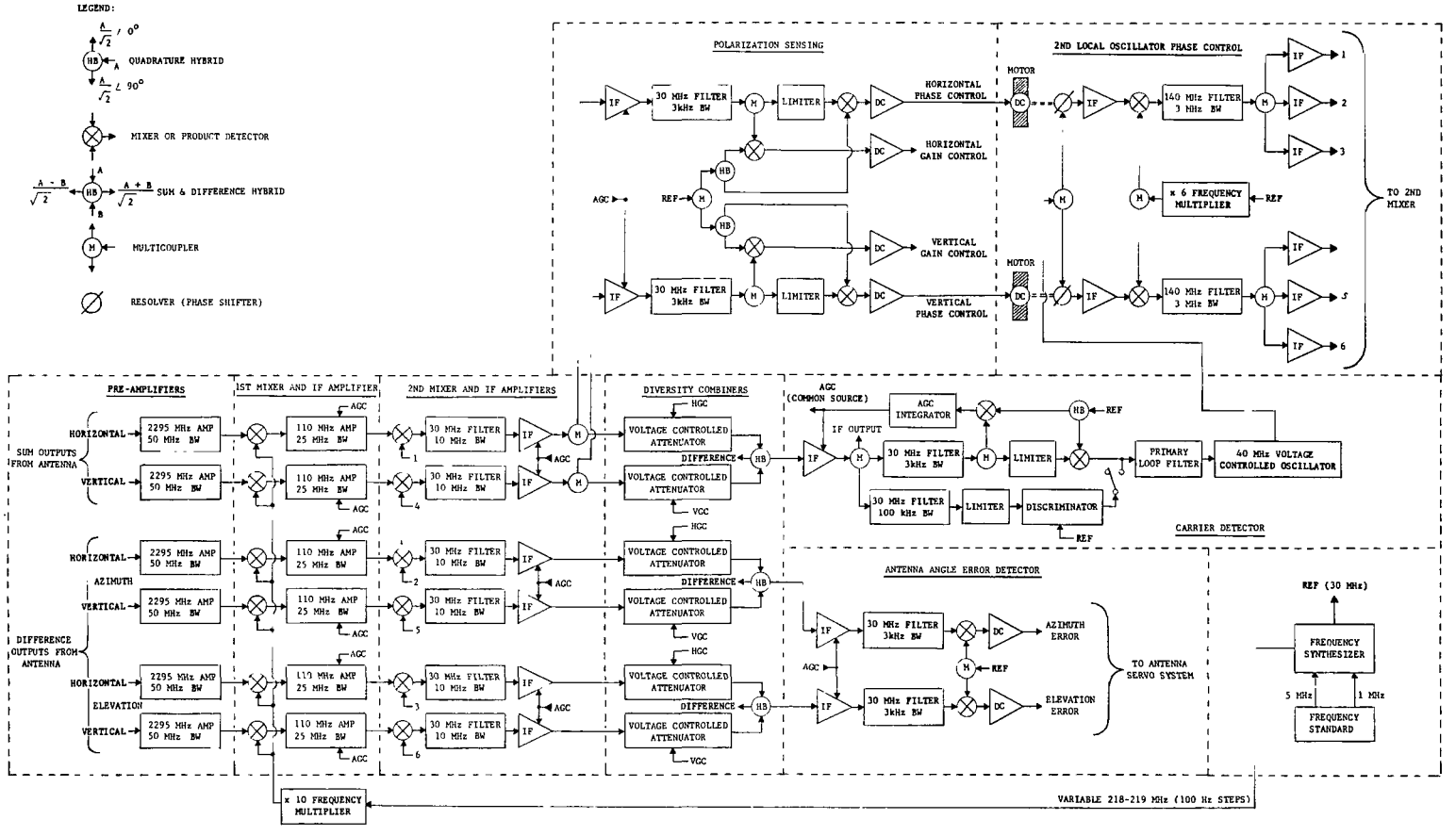

Figure 1.- Predetection, polarization diversity combiner.

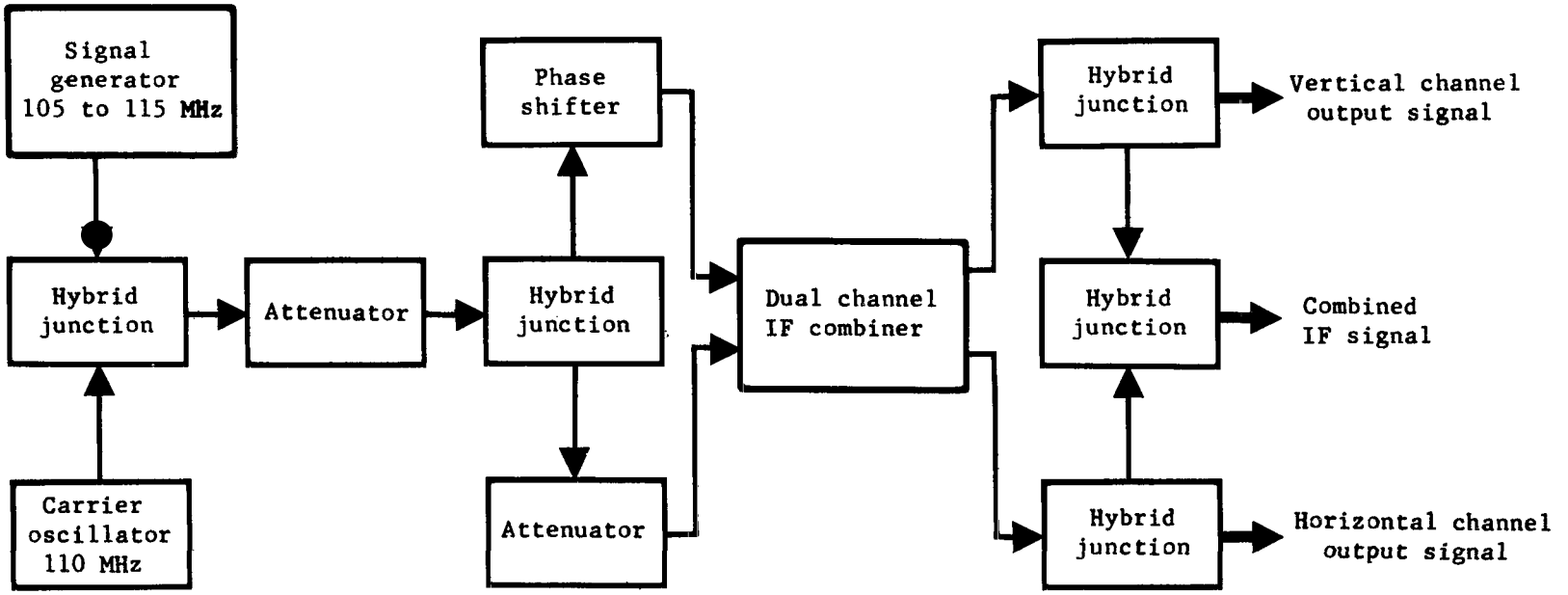

Figure 2.- Equipment configuration for evaluating IF combiner.

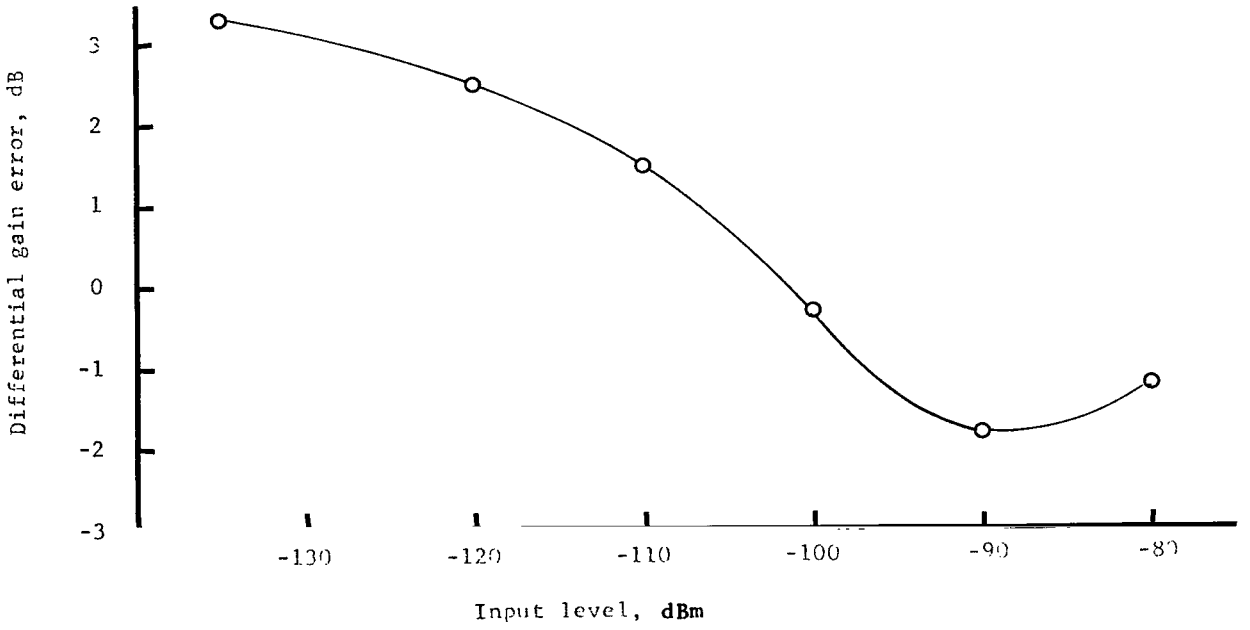

Figure 3.- Variation of gain mismatch with input signal level.

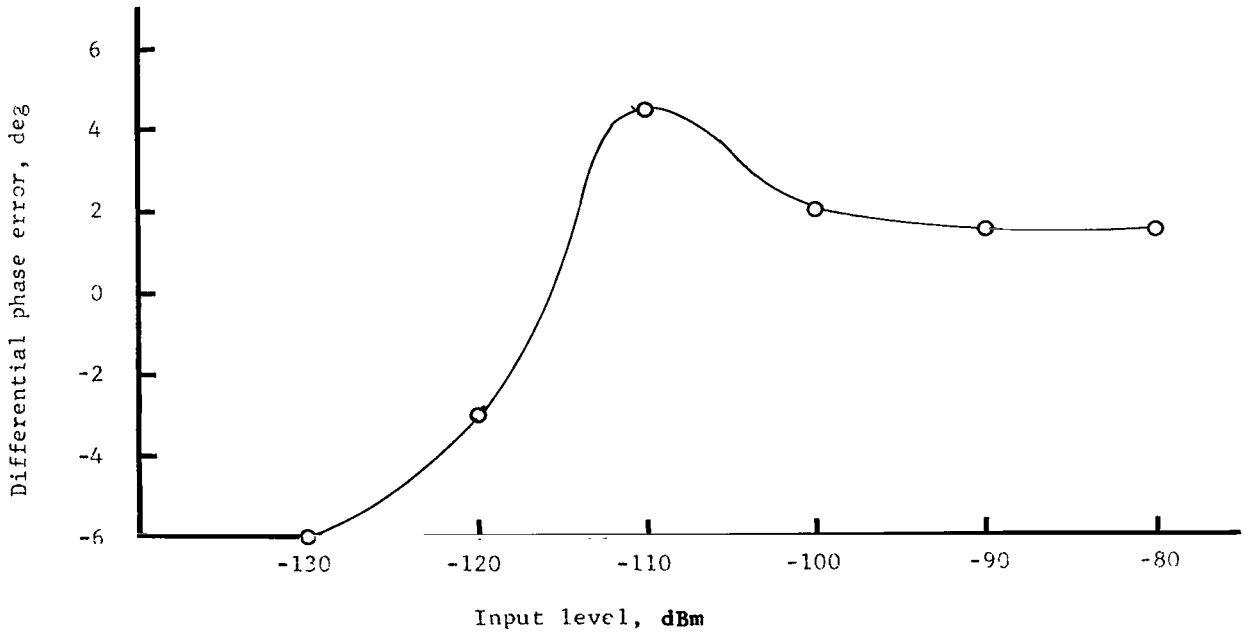

Figure 4.- Variation of phase mismatch with input signal level.

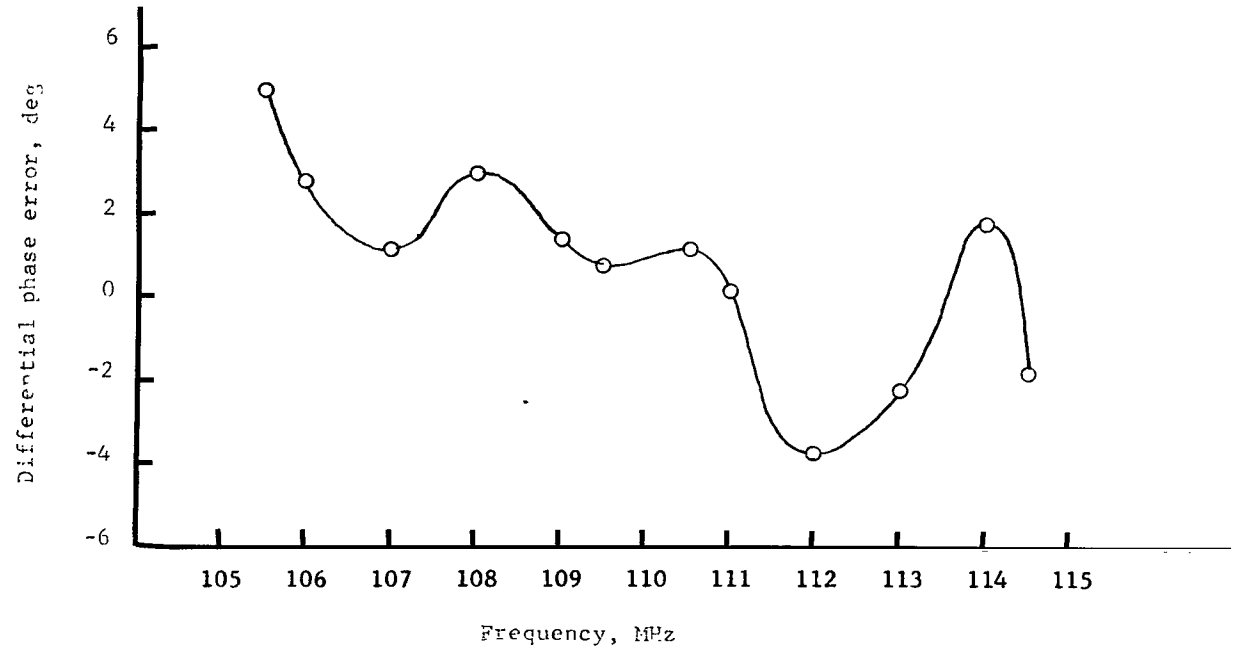

Figure 5.- Variation of phase error with frequency.

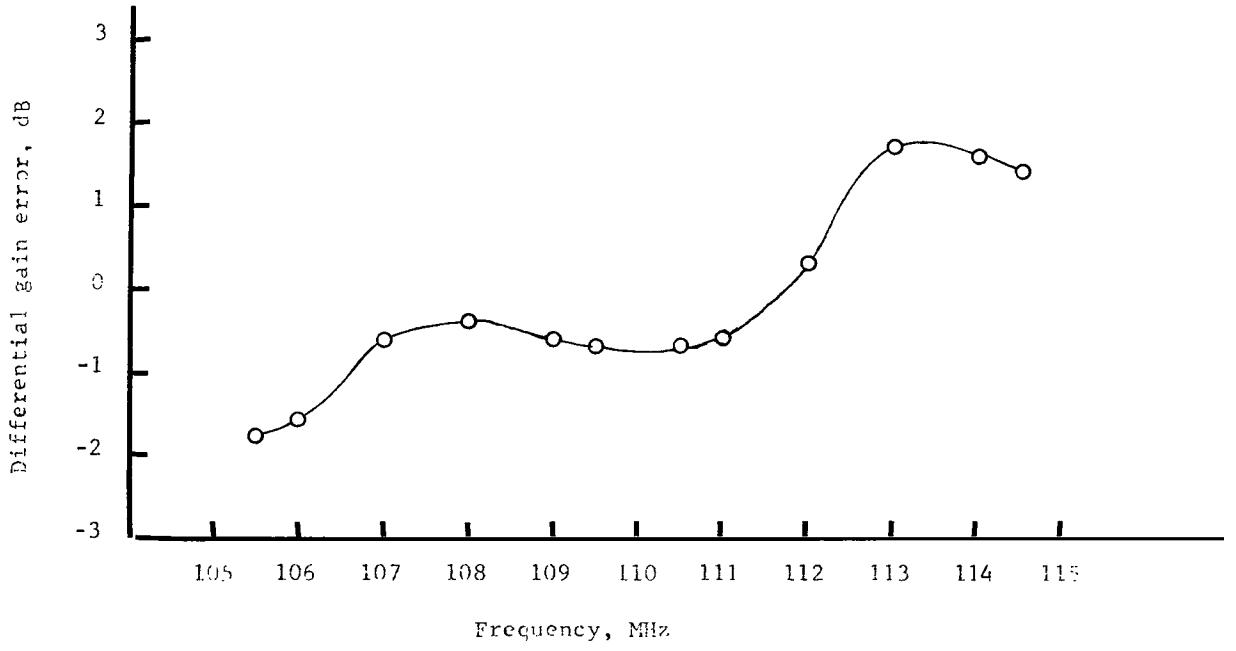

Figure 6.- Variation of gain error with frequency.

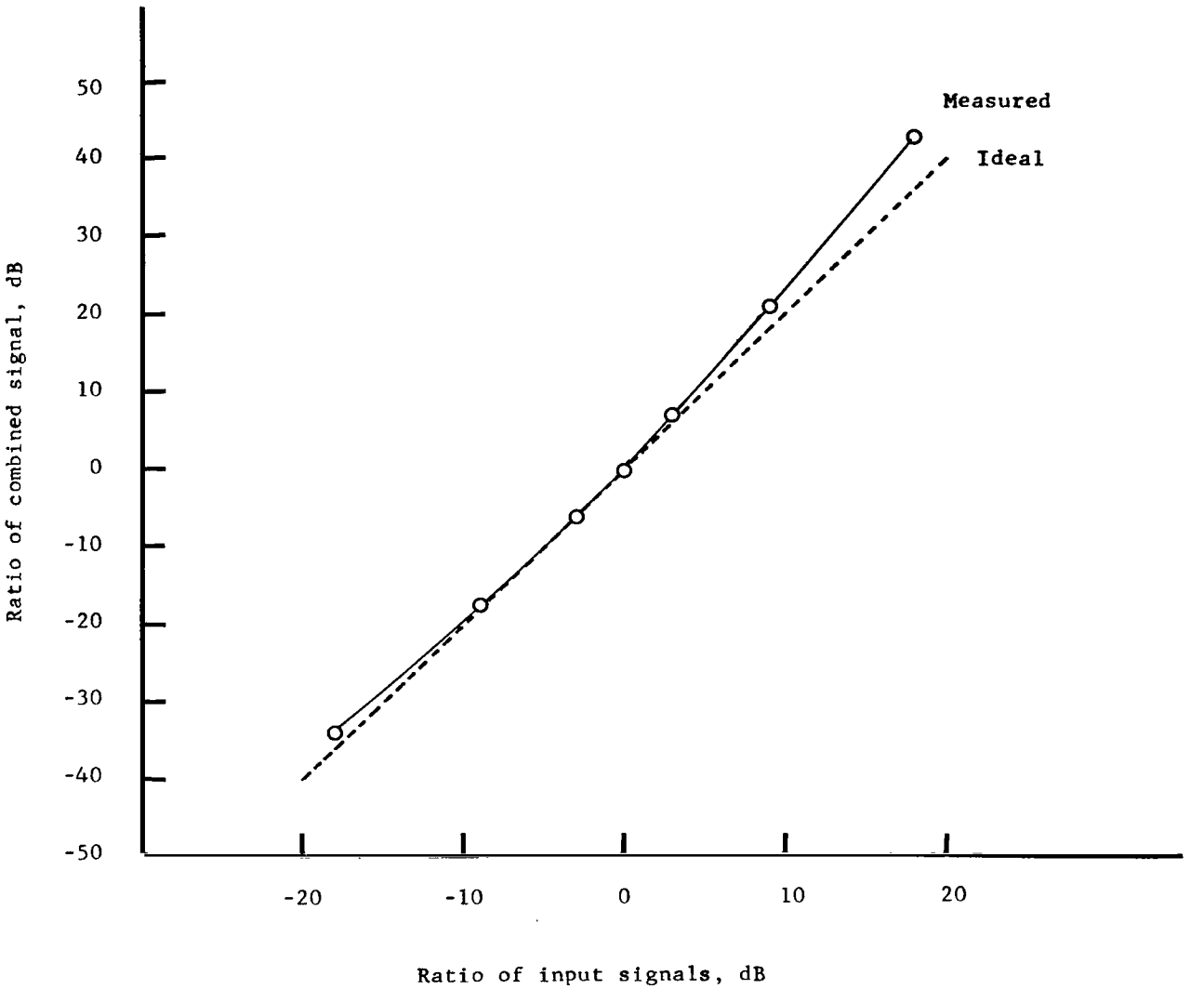

Figure 7.- Variation of weighting accuracy with input signal level.

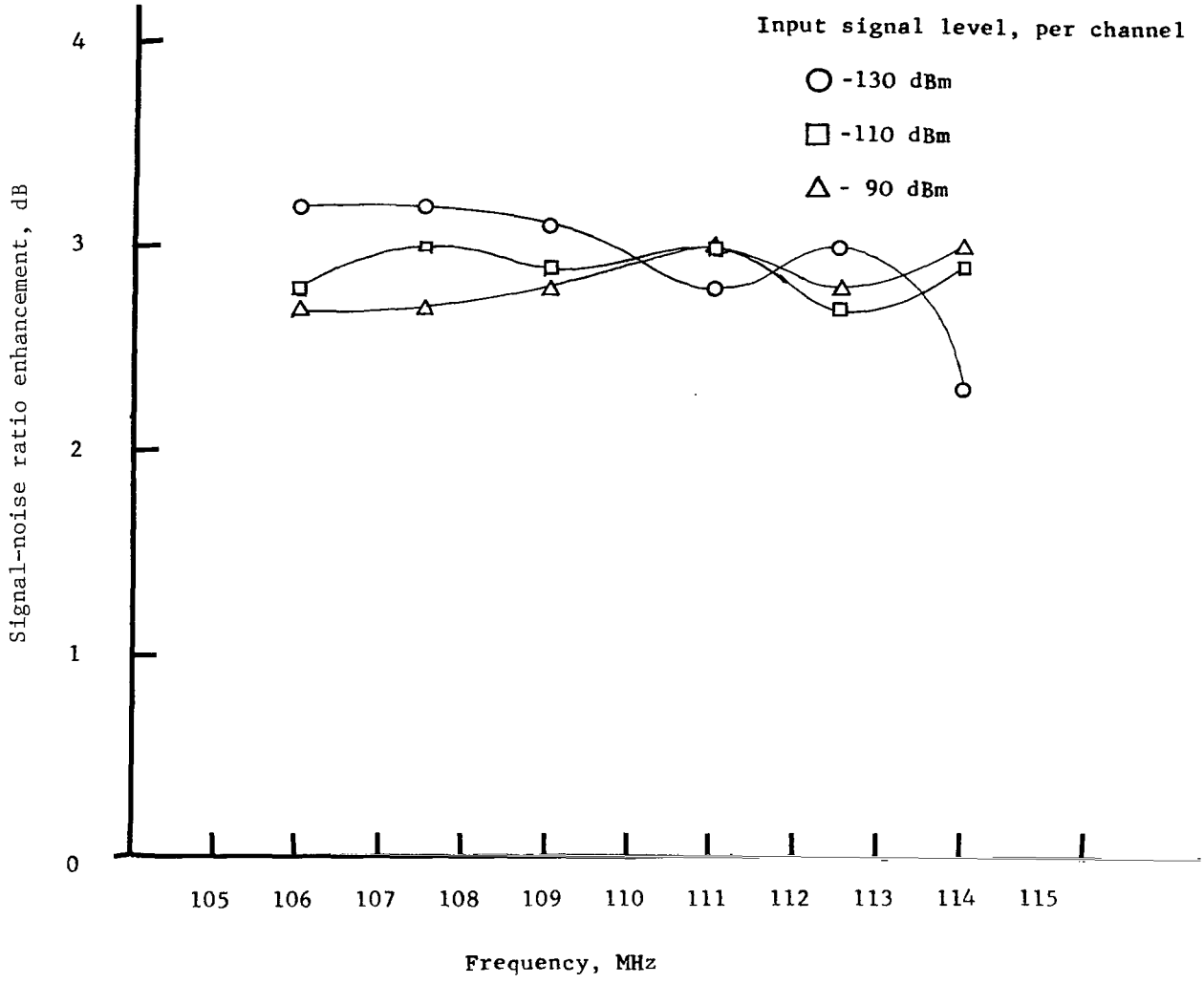

Figure 8.- Variation of combination efficiency with frequency.

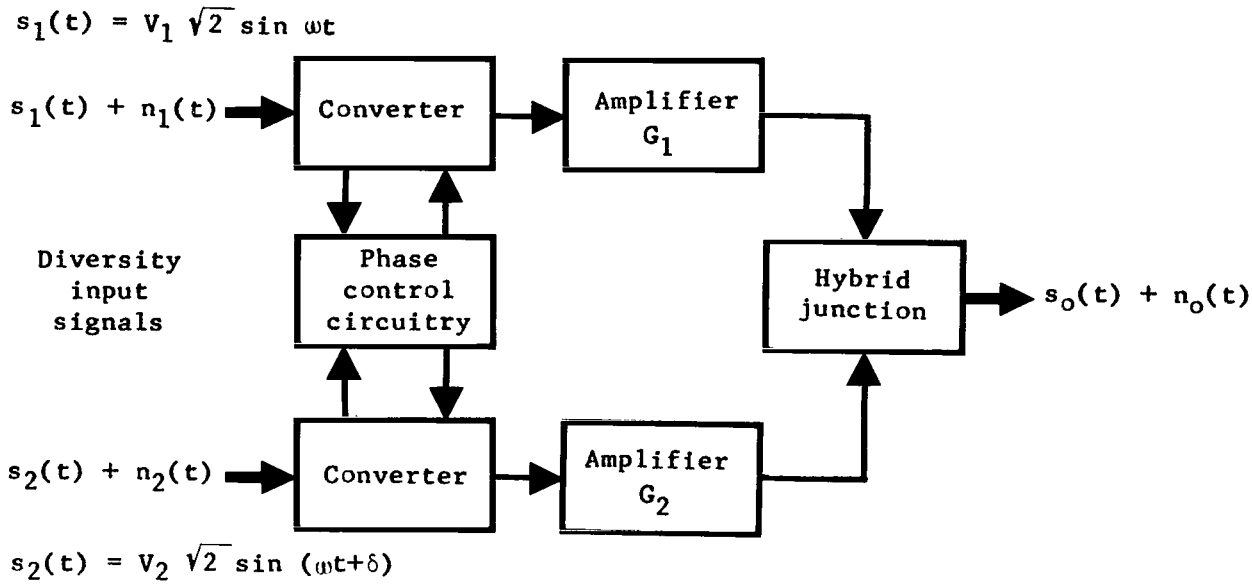

Figure 9.- Gain-weighted summation of diversity signals.

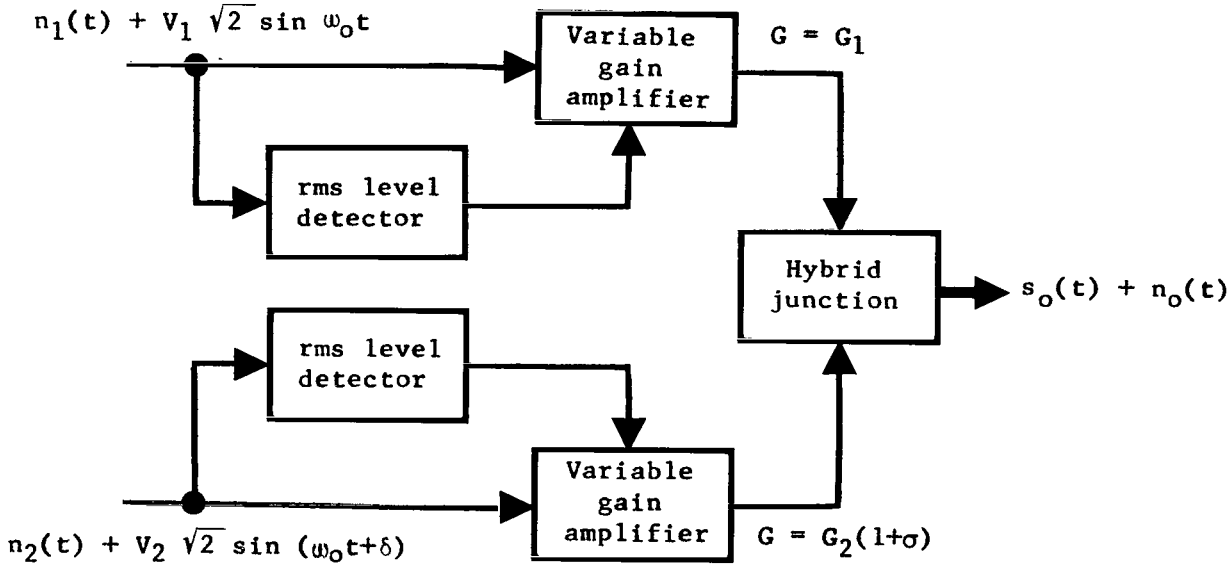

Figure 10.- Nonideal maximal ratio combination.

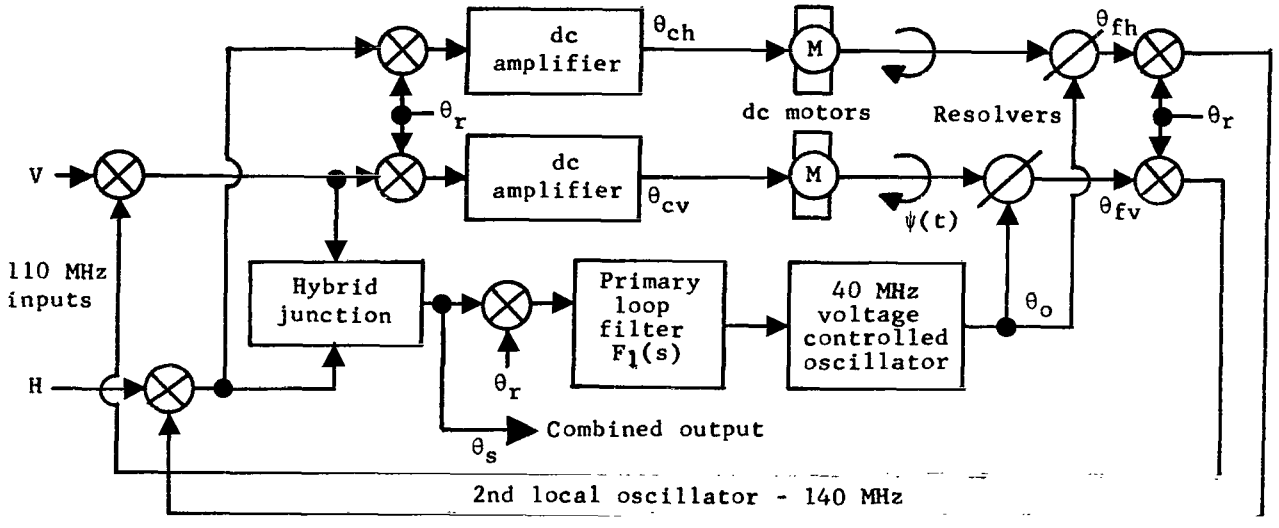

Figure 11.- Sum channel functional diagram for equal amplitude weighting.

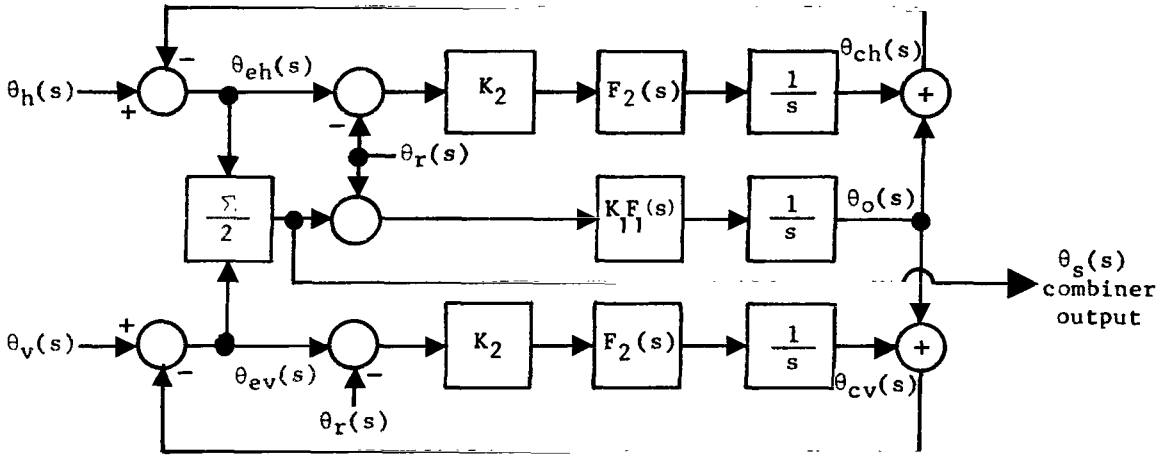

Figure 12.- Linearized phase equivalent circuit for carrier tracking loops. (Equal input signal amplitudes.)

NASA-Langley, 1970 — 7 L-7057

"The aeronautical and space activities of the United States shall be conducted so as to contribute . . . to the expansion of human knowledge of phenomena in the atmosphere and space. The Administration shall provide for the widest practicable and appropriate dissemination of information concerning its activities and the results thereof."

—NATIONAL AERONAUTICS AND SPACE ACT OF 1958

NASA SCIENTIFIC AND TECHNICAL PUBLICATIONS

TECHNICAL REPORTS: Scientific and technical information considered important, complete, and a lasting contribution to existing knowledge.

TECHNICAL NOTES: Information less broad in scope but nevertheless of importance as a contribution to existing knowledge.

TECHNICAL MEMORANDUMS: Information receiving limited distribution because of preliminary data, security classification, or other reasons.

CONTRACTOR REPORTS: Scientific and technical information generated under a NASA contract or grant and considered an important contribution to existing knowledge.

TECHNICAL TRANSLATIONS: Information published in a foreign language considered to merit NASA distribution in English.

SPECIAL PUBLICATIONS: Information derived from or of value to NASA activities. Publications include conference proceedings, monographs, data compilations, handbooks, sourcebooks, and special bibliographies.

TECHNOLOGY UTILIZATION PUBLICATIONS: Information on technology used by NASA that may be of particular interest in commercial and other non-aerospace applications. Publications include Tech Briefs, Technology Utilization Reports and Notes, and Technology Surveys.

Details on the availability of these publications may be obtained from:

SCIENTIFIC AND TECHNICAL INFORMATION DIVISION

NATIONAL AERONAUTICS AND SPACE ADMINISTRATION

Washington, D.C. 20546